Iranian Journal of Catalysis 6(3), 2016, 281-292

IRANIAN JOURNAL OF CATALYSIS

Photocatalytic self-cleaning properties of lanthanum and silver co-doped TiO_2 nanocomposite on polymeric fibers

Hadi Fallah Moafi*

Department of Chemistry, Faculty of Science, University of Guilan, P.O. Box 41635-1914, Rasht, Iran.

Received 3 April 2016; received in revised form 27 May 2016; accepted 7 June 2016

ABSTRACT

Titania, single-doped and lanthanum-silver co-doped titania nanocomposite were coated on cellulosic and polyacrylonitrile fibers *via* sol–gel method. The prepared samples were evaluated using x-ray diffraction (XRD), scanning electron microscopy (SEM), energy dispersive x-ray spectroscopy (EDX), transmission electron microscopy (TEM), X-ray photoelectron spectroscopy (XPS), photoluminescence spectroscopy (PL) and BET surface area measurement. The photo self-cleaning activity of the nanocomposites coated-fibers were determined by degradation of methylene blue and eosin yellowish under UV-Vis light. Diffuse reflectance spectroscopy was used to monitor photodegradation of dyes. The results of EDX and XPS revealed that La and Ag was doped into TiO_2 structure. The results of EDX, TEM and BET analyses indicated that the TiO_2 and TiO_2 nanocomposite coatings were composed of nanoparticles or aggregates with a size of less than 20 nm. All samples demonstrated photocatalytic self-cleaning properties when exposed to UV-Vis irradiation. The results showed that the La^{3+}/Ag^{+} co-doping is more beneficial than single doping of TiO_2 coating and the synergistic effect of La^{3+} and Ag^{+} is responsible for improving the photo-activity. This may be ascribed to the microstructure of TiO_2 and the effect of the doping modes on the structural and electronic properties of the anatase phase.

Keywords*: La-Ag co-doped titania nanocomposite; Photocatalytic self-cleaning; Sol-gel; Cellulosic fibers; Polyacrylonitrile fibers.*

1. Introduction

The potential applications of metal oxide semiconductors to environmental remediation have attracted extensive attention because of their outstanding physical and chemical properties. Among the reported photocatalysts, titanium dioxide (TiO_2) has been widely studied as a photocatalyst due to its remarkable features including low cost, chemical stability, non-toxicity, favorable optoelectronic properties, strong oxidizing abilities for the decomposition of organic pollutants and high photocatalytic activity [1-3]. Development of photo-induced self-cleaning materials is one of the most important applications of photocatalytic properties of oxide semiconductors. Metal oxide semiconductor such as titanium dioxide has the ability to decay organic pollutants on its surface through photocatalysis in the presence of UV-light and an oxygen source.

*Corresponding author emails: fallah.m@guilan.ac.ir, h.f.moafi@gmail.com
Tel./Fax: +98 13 3336 7262

Nontoxic and inexpensive nano anatase TiO_2 immobilized on surface of materials such as glass, polymeric and textile materials for photocatalysis and self-cleaning purpose have been achieved [4-12].

Besides the photo self-cleaning properties, TiO_2 is also prominent for its photo-induced super-hydrophilic, high refractive index and transmittance as well as remarkable abrasive resistance and chemical stability. Self-cleaning performance has also been described for super hydrophilic films with photoactive nanoparticles such as TiO_2 [4,13,14]. Unfortunately, though TiO_2 is a good photocatalyst, TiO_2 has several disadvantage and shows activity only under UV light excitation because of its wide band gap that limits TiO_2 use under visible light [15,16]. Furthermore, TiO_2 presents a relatively high electron-hole recombination rate which is unfavorable to its photoactivity. Therefore, suppression of the recombination of photo-generated electron/hole pairs in the TiO_2 is essential for improving the efficiency of photocatalytic activity.

In order to improve the photocatalytic activity of TiO_2 and other oxide semiconductor, many nonmetal ions

[17-19], transition metals [20-24], noble metals [15,25,33,34] and lesser band gap semiconductors [35] were doped into TiO_2 nanocrystals to inhibit the recombination of photo-induced electrons and holes and also to enhance the optical adsorption in the visible region. Transition metals and noble metal ions doping into the oxide semiconductors have shown a significant decrease in band gap energy (Eg) and enhanced the charge separation of charge carriers. In particular, loading TiO_2 with noble metals (e.g., Pt, Au or Ag) has proved to be an effective dopant to enhance the photocatalytic efficiency of TiO_2. They may extend the light absorption into the visible range and enhance electron excitation by surface plasmon resonances (SPR) and modify the surface properties of photocatalysts [15]. Recently, simultaneous incorporation of multi-dopants (co-doping process) has received much more attention to improve the photoactivity of wide band gap semiconductors such as TiO_2 [36-47]. Doping TiO_2 with multiple ions can lead to a lower band gap and as a result improve the visible light use of TiO_2. Double element co-doped TiO_2 system shows higher photocatalytic activity compared to the mono-doped TiO_2, and some of the co-doping elements have synergistic effects in the photocatalytic experiments [42-47].

The current study presents a facile and effective design of a hybrid nanocrystalline La-Ag/TiO_2 coating on cellulosic and polyacrylonitrile fibers. Self-cleaning properties have been realized by depositing TiO_2, Ag-TiO_2, La-TiO_2 and La-Ag-TiO_2 coatings onto fiber substrates using a combined sol–gel dip-coating process. The performance of the designed TiO_2 nanocomposites as photoactive hybrid materials was investigated by evaluating of physicochemical properties and photocatalytic activity.

2. Experimental

2.1. Reagents and materials

All commercial reagents such as titanium tetrabutoxide (TTBO), lanthanum nitrate hexahydrate, silver nitrate, acetic acid, methylene blue and eosin yellowish were analytically pure, and were purchased from Merck (Germany) and used without further purification. The used cellulosic and polyacrylonitrile fibers were 100% woven fabric, plain construction, with a density of 144 $g.m^{-2}$ and 180 $g.m^{-2}$, respectively. The fibers were washed first by water and detergent at 80°C for 30 min to remove the impurities and chemical residues. Then, there were washed several times by de-ionized water and dried at 25°C for 24 h.

2.2. Synthesis procedure

The sol–gel method was used for the preparation of TiO_2, doped and co-doped TiO_2 nanocomposites. In a typical procedure route for preparation of the TiO_2 sol, 15 ml of TTBO was added to acetic acid (30 ml) and stirred for 0.5h and then de-ionized water was added to the mixture dropwise with vigorous stirring. The solution was stirred for 2 h to achieve a clear transparent sol. For making of La-TiO_2 sol, a certain amount of lanthanum nitrate hexahydrate (0.382 g) was dissolved in deionized water (60 ml) and was then added into the mixture of TTBO and acetic acid dropwise with vigorous stirring for 1h.

For preparation of Ag-TiO_2, the required amount of silver nitrate (0.15 g) was treated the same way as described for La-TiO_2. These solutions were stirred for 2 h to get a clear transparent doped titania sol. In the synthesis procedure of La-Ag co-doped titania sol, silver nitrate (0.075 g) and lanthanum nitrate hexahydrate (0.191 g) were dissolved into deionized water under vigorous stirring and then the solution was added into the mixture of TTBO and acetic acid dropwise with vigorous stirring at room temperature. The obtained co-doped TiO_2 nanosol was stirred for 2h to obtain a clear sol and ready for coating procedure.

The dip-pad-dry-cure process was employed to apply the as-prepared sols onto the fibers for preparation a durable layer. The cellulosic and polyacrylonitrile fabrics were immersed in the TiO_2 and doped co-doped TiO_2 hydrosols for 5 min and then padded with a horizontal roller. The coated substrates were heated for 30 min at 80°C in preheated oven and then cured at 150°C for 5 min to complete the formation of titania and titania nanocomposites. Finally, the fabrics were immersed in 80°C hot water for 1h. During this step, the unattached particles were removed from the fabric surface.

2.3. Photocatalytic activity measurements

The UV-Vis light photocatalytic activity of coated-fibers was evaluated by studying of the photodegradation of Methylene Blue (MB) and Eosin Yellowish (EY). Irradiations were carried out using a UV-Vis light Mercury lamp (high pressure lamp, HPMV 400W, Germany) with maximum emission at 365 nm without filter, which was placed vertically in the reactor. The lamp yields a spectrum ranging from ultraviolet to visible light (200-800 nm). Details of the experimental procedure were described in our previous work [5,6]. The photocatalytic decomposition was determined from the following equation:

$$Photocatalytic\ decomposition = (C_o\text{-}C)/C_o$$

The photocatalytic reaction kinetics follows Langmuir-Hinshelwood model. The simplified equation could be represented as follows:

$$ln(C/C_o) = -kt$$

Where k is the first-order reaction rate constant, t is reaction time, C_o the initial concentration of the dyes on fiber surface, and C the final concentration after

illumination by light. The concentration of dyes was calculated by standard calibration curve. The calibration measurement was performed to correlate the concentration between the different known concentrations of 1×10^{-6} - 5×10^{-5} M and the absorbance of MB (λ_{max}=665) and EY (λ_{max}=565).

2.4. Materials characterization

X-ray diffraction pattern of samples was carried out at room temperature with D8 Bruker X-ray diffractometer with Cu-Kα radiation, scan rate 0.022θ/s and within a range of 2θ of 10 to 70 degrees. The sample morphology observations were recorded by scanning electron microscopy (SEM, Philips XL30) equipped with an EDS attachment for compositional analysis. Transmission electron microscopy (TEM) images were taken from a Philips CM10 transmission electron microscopy with an accelerating voltage of 100 kV. For surface chemical analysis, X-ray photoelectron spectroscopy (XPS) was performed on samples with 8025-BesTec twin anode XR3E2 x-ray source system. Photoluminescence spectra (PL) of the samples were measured with Hitachi F-7000 fluorescence spectrophotometer. For evaluation of photodecomposition reaction, the UV–Vis spectra were recorded at room temperature by a UV-2100 Shimadzu spectrometer in the reflectance mode by evolution of the absorbance. The BET surface area of the samples was determined by Sibata SA-1100 surface area analyzer.

3. Results and Discussion

3.1. XRD analysis

The XRD patterns of pure fibers, TiO_2, doped and co-doped TiO_2 coated-fibers and sol-obtained powders are reported in Figs. 1 to 3. In Figs. 1 and 2, the typical XRD reflections of the cellulosic and polyacrylonitrile fibers were identified. Fig. 1a shows two broad peaks at 13.16°, 15.12° and one intense peak at 21.4°, which comprise the typical XRD pattern of cellulosic fibers [48]. Fig. 2 (peak a) shows two peaks: the intense one at 17° and the broad one at 29°, which constitute the typical XRD pattern of PAN fibers [49]. Figs. 1b-1e and Figs. 2b-2e show the XRD patterns of TiO_2-coated, Ag-dopedTiO_2, La-doped TiO_2 and La-Ag co-doped coated fibers. Since the amount of TiO_2 doped and co-doped TiO_2 were low on the fibers surface, the XRD patterns of TiO_2, doped and co-doped TiO_2-coated fibers illustrate a low intensity of anatase phase reflections. The reflections apperceived at 2θ= 25°, 37°, 48° and 55° and 62° are related to anatase phase.

Fig. 3 shows XRD patterns of sol–gel derived TiO_2, Ag-doped TiO_2, La-doped TiO_2, and La-Ag co-doped TiO_2 powders. It can be observed that all reflections related to anatase phase and no other reflections of other phases such as rutile and brookite are observed.

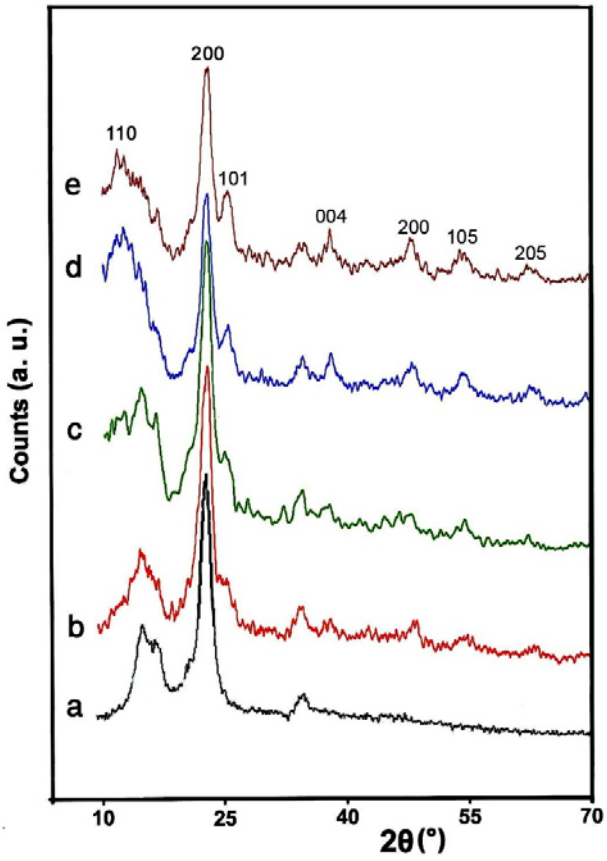

Fig. 1. XRD patterns of: (a) pure cellulosic fiber, (b) TiO_2 coated fiber, (c) Ag-TiO_2 coated fiber, (d) La-doped TiO_2 coated fiber, and (e) La-Ag-TiO_2 coated fiber.

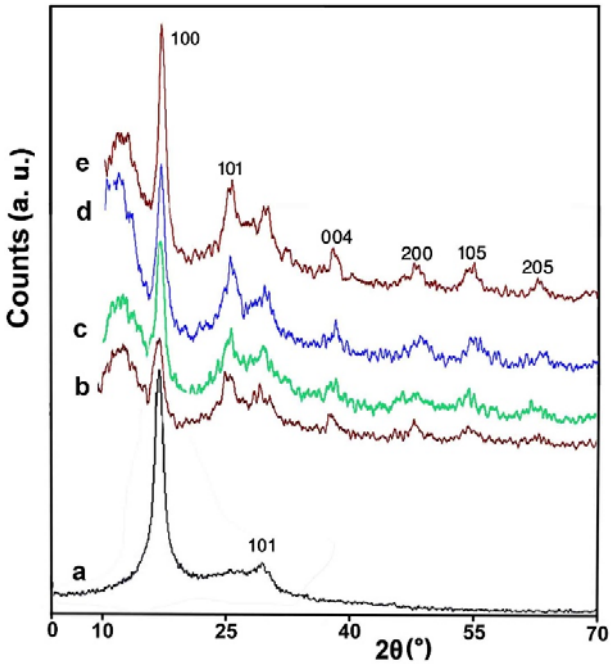

Fig. 2. XRD patterns of: (a) pure polyacrylonitrile fiber, (b) TiO_2 coated fiber, (c) Ag-TiO_2 coated fiber, (d) La-doped TiO_2 coated fiber, and (e) La-Ag-TiO_2 coated fiber.

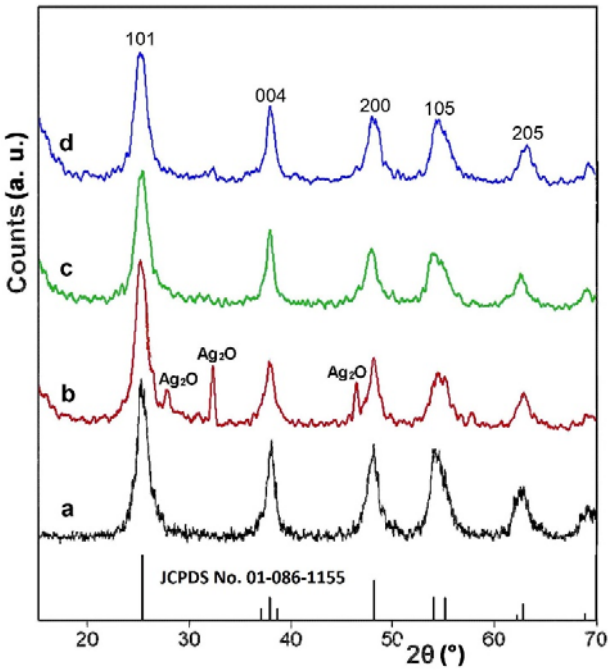

Fig. 3. XRD patterns of sol-derived powders: (a) TiO_2, (b) Ag-doped TiO_2, (c) La-doped TiO_2 and (d) La-Ag -co-doped TiO_2.

On the other hand, all prepared samples showed XRD peaks related to anatase crystaline structure that was very similar to what was previously reported as JCPDS No. 01-086-1155. These observations indicate that there is virtually no phase change in TiO_2 structure and crystallinity in the process of doping or co-doping. In Fig. 3b, the peaks at $2\theta = 27.90°$, 32.28° and 46.36° are related to (110), (111) and (211) planes of face-centre cubic of Ag_2O [50,51]. Ag_2O is unstable under light irradiation and decomposes into metallic Ag particles during the photocatalytic decomposition of dyes. However, after partial in situ formation of Ag on the surface of Ag_2O, the Ag_2O-Ag composite can work as an efficient photocatalyst [52].

The relatively high width of the reflections suggests that the size of the particles is quite small. It is observed that doping of La and Ag reduced the grain size and enlarged the surface areas of nanoparticles. The average grain size of nanoparticles is estimated using the Scherrer's equation based on the full width at half-maximum (FWHM) of the (101) peak of the samples (Table 1). The crystallite size, on the other hand, has been reduced with the doping process as signified by the peak broadening in the XRD patterns of Ag-TiO_2 and La-TiO_2 (Table 1). TiO_2 and the doped TiO_2 nanoparticles were prepared in presence of acetic acid. Protonation of TiO_2 nanoparticles can prevent further crystallization. Furthermore, the surplus acetate anion adsorbed on the surface of TiO_2 could also prevent the growth of nano TiO_2. This role of acetate anion on the surface of TiO_2 could be responsible for the decrease in the crystallite size of TiO_2 during the sol–gel synthesis [53].

3.2. Morphological and compositional analysis

The microscope morphologies of the as-prepared TiO_2 and doped TiO_2 fibers were investigated by SEM observation (Figs 4 and 5). Figs. 4a and 5a show the surface of the pristine fibers. Fig. 4a shows that the surface of pristine cellulosic fiber is clean and smooth. In Fig. 5a, the surface of the fibers is relatively smooth, and the groove-like structure on the PAN fibers surfaces seems clear. Figs 4b and 5b show the treated fibers with TiO_2 coating. They are covered by continuous and dispersed TiO_2 nanoparticles which are composed of aggregates of an anatase nanostructure. Figs 4c and 5c show the treated fibers with Ag-TiO_2 nanosols. Ag-TiO_2 coated-fibers show a surface morphology similar to that of the bare TiO_2 coating. It can be observed that the deposited nanoparticles on fibers were composed of agglomerates of Ag-TiO_2 nanoparticles. The SEM images of the treated fibers with La-doped TiO_2 are shown in Figs 4d and 5d. These Figs. indicate that shape of the nanoparticles is analogous to other samples and were constructed of agglomerates of irregularly nanoparticles. Lastly, Figs 4e and 5e is low-magnification SEM image of the La-Ag-TiO_2 coated-fibers, whose surface has been covered with a large number of La-Ag-TiO_2 particles, which show agglomeration of La-Ag-TiO_2 nanocomposite with nanometer dimensions.

The elemental analysis of the treated samples with La-Ag-TiO_2 was performed by EDAX analysis. Results are shown in Fig 6.

Table 1. Some characteristics of synthesized nano TiO_2 and TiO_2 nanocomposite coating

Crystalline structure	Samples (deposited on the fibers)	*K(rate constant)*				BET surface area (m^2/g)	Pore volume (cm^3/g)	XRD crystal size (nm)	TEM crystal size (nm)
		Cell		PAN					
		MB	EY	MB	EY				
Anatase	TiO_2	0.114	0.186	0.182	0.194	350	0.125	20	10-15
Anatase	Ag-TiO_2	0.152	0.241	0.207	0.245	372	0.132	8	<5
Anatase	La-TiO_2	0.176	0.296	0.244	0.295	290	0.103	8	<10
Anatase	La-Ag-TiO_2	0.222	0.347	0.334	0.337	318	0.113	15	5-10

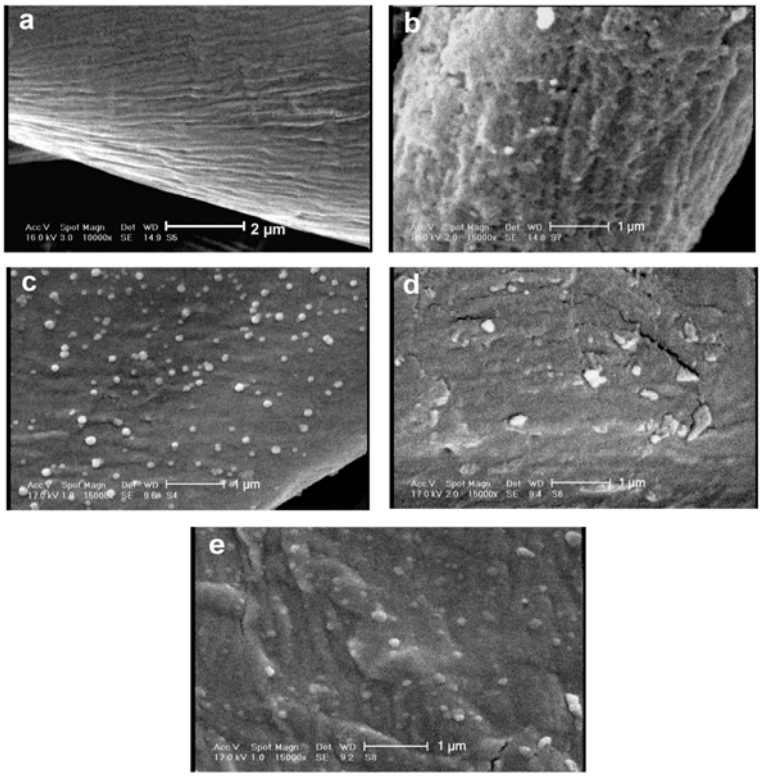

Fig. 4. SEM images of: (a) pure cellulosic fiber, (b) TiO_2-coated fiber, (c) Ag-TiO_2-coated fiber, (d) La-TiO_2-coated fiber and (e) La-Ag-TiO_2-coated fiber.

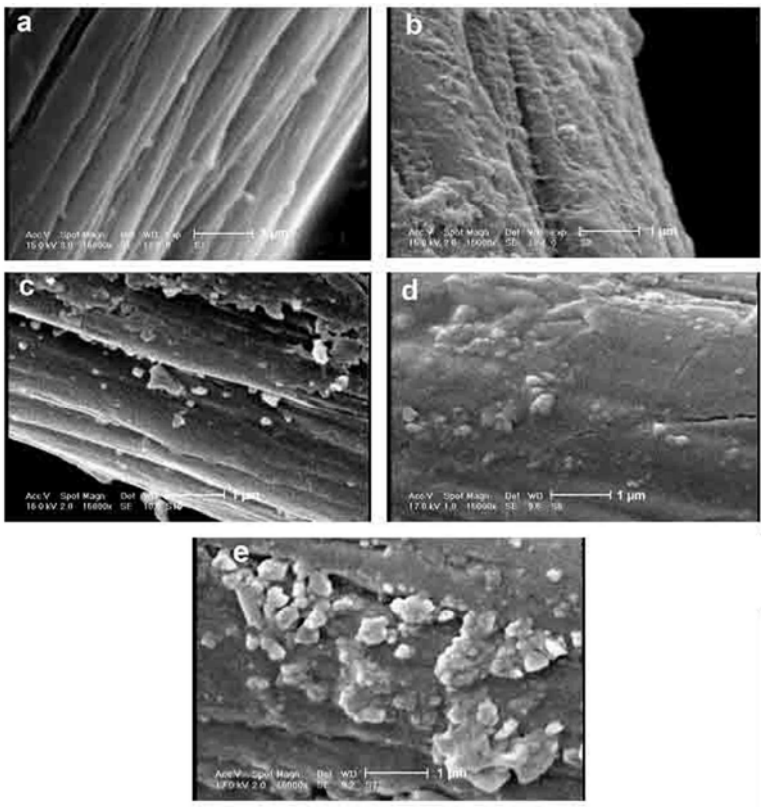

Fig. 5. SEM images of: (a) pure polyacrylonitrile fiber, (b) TiO_2-coated fiber, (c) Ag-TiO_2-coated fiber, (d) La-TiO_2-coated fiber and (e) La-Ag-TiO_2-coated fiber.

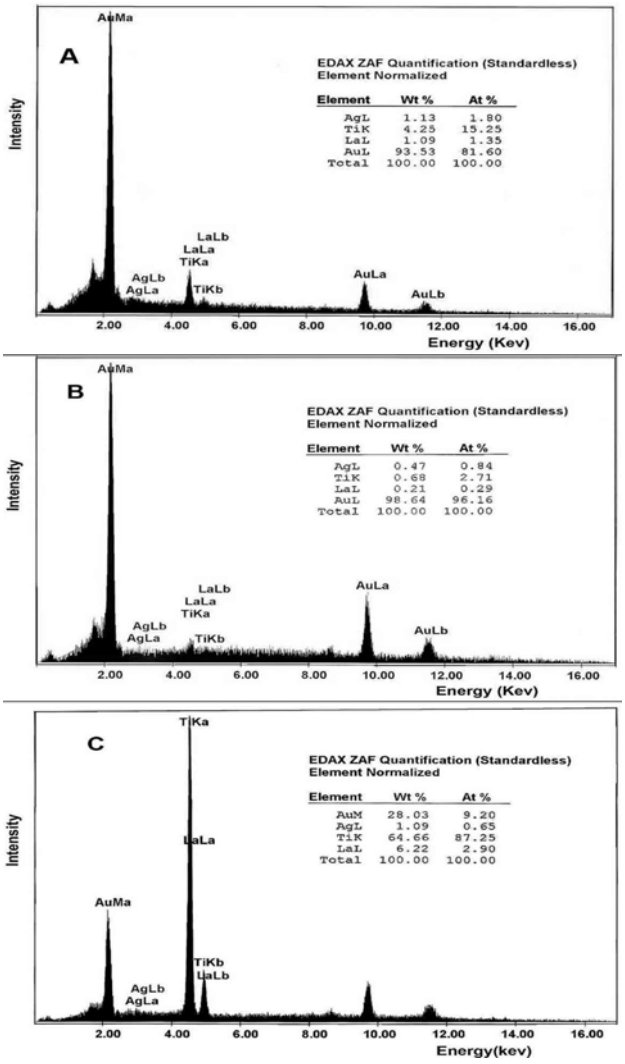

Fig. 6. EDAX analysis of: (a) La-Ag-TiO_2 coated cellulosic fiber, (b) La-Ag-TiO_2 coated polyacrylonitrile fiber, (c) La-Ag-TiO_2 nanocomposite powder.

According to the EDAX analysis, the amount of Ti and other elements slightly varies, meaning that doping ions are located in the crystal structure. It is noteworthy to mention that after washing process, remarkable amount of TiO_2 and doping ions are still present on the fibres surface and TiO_2 nanocomposites have sufficient adhesion towards the fibers.

Fig. 7 shows TEM micrographs of the TiO_2 and TiO_2 nanocomposite samples on the fibers. TEM image of TiO_2 on the coated fibers (Fig. 7a) show that the deposited titania consists of nanoclusters with an average size of ~10-15 nm, which is consistent with the XRD result. The TEM image of Ag-TiO_2 on the surface of the fibers shows that the size of Ag-TiO_2 particles are much smaller than deposited titania, mostly less than 5 nm, as seen in Fig 7b. For Ag–TiO_2 sample, Ag species are well dispersed on the TiO_2 nanoparticles and their size distribution demonstrates that most of them are in the 30–40 nm range.

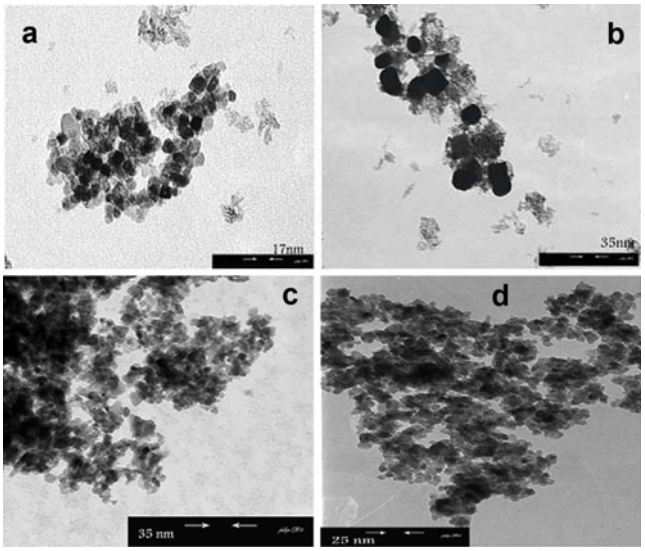

Fig. 7. TEM images of: (a) TiO_2 on fibers, (b) Ag-TiO_2 nanocomposite on fibers, (c) La-TiO_2 nanocomposite on fibers, and (d) La-Ag-TiO_2 nanocomposite on fibers.

The small size of silver and TiO_2 nanoparticles suggests that the exposed surface area of Ag-TiO_2 coating is very large. Fig. 7c shows that La-doped TiO_2 sample consists of the agglomerates of primary particles with an irregular shape and size of nanoparticles less than 10 nm, which is in good agreement with XRD data. Indeed, it is demonstrated that Ag and La doping could inhibit the increase of TiO_2 particle size. The shape of the La-Ag co-doped TiO_2 nanoparticles was observed as less aggregated nanoparticles with an average particle size of 5-10 nm (Fig 7d). The La–Ag co-doped sample had better dispersibility than undoped TiO_2, and the particle size was smaller. On the other hand, aggregation among nanocrystallites could decrease during co doping treatment.

3.3. Photoluminescence (PL) emission study

In order to investigate the electron–hole recombination feature, photoluminescence (PL) studies were carried out. Photoluminescence (PL) emission is a helpful method to specify the trapping and migration efficiency of electron–hole pairs, and to recognize the behavior of the charge carriers [40]. The PL spectra of TiO_2, Ag-doped TiO_2, La-doped TiO_2, and La-Ag-co-doped TiO_2 are illustrated in Fig. 8. The samples display strong peaks around 400 and 465 nm under the excitation at 280 nm. The former is due to the free-excitation emission of the band gap [40,54]. The latter is attributed to the charge-transfer transition from Ti^{3+} to oxygen anion in a TiO_6 octahedral complex. It was found that the spectrum of the prepared pure TiO_2 and doped TiO_2 photocatalysts were similar, but the PL intensity was different. The PL spectra show oxygen vacancies or other point defects present in the photocatalyst.

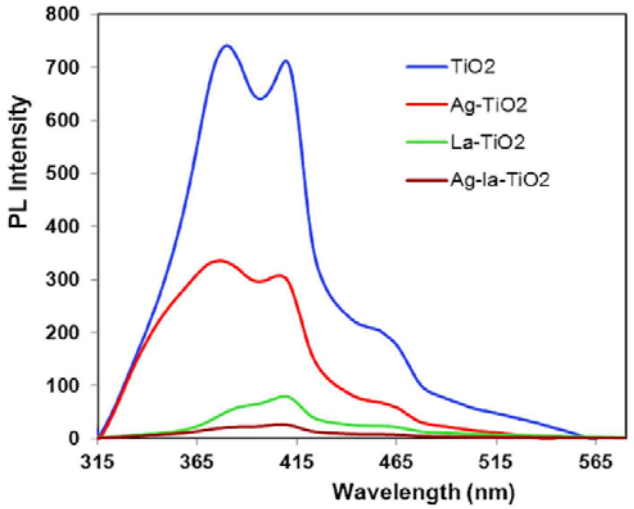

Fig. 8. Photoluminescence spectra of TiO_2, Ag-TiO_2, La-TiO_2 and La-Ag-TiO_2 nanocomposite.

Since PL emission results from the recombination of excited charge carriers, so low PL intensity demonstrates a low recombination rate of excited electrons and holes. As shown in Fig. 8, the prepared La-Ag co-doped TiO_2 had a lower recombination rate of electrons and holes than the pure TiO_2 and single doped TiO_2. These results indicate that the recombination of photo-generated electrons and holes is effectively suppressed by co-doping, and TiO_2 sample co-doped by La and Ag shows a better ability of separating photo-induced charge carriers than the single doped, which may lead to higher photocatalytic activity. In contrast to pure TiO_2, the decrease in emission intensity originates from the differences in electronic structure of the metal doped samples, where some new defects will form, such as oxide ion vacancy [40].

3.4. XPS study

X-ray photoelectron spectrum (XPS) is a powerful technique for the investigation of electron structure to characterize the oxidation state, the chemical nature, the valance states, and composition of atom on the surface of materials. The XPS spectra of La-Ag-TiO_2 are shown in Fig. 9 and Fig. 10. The XPS spectrum (Fig. 9) shows that the main elements on the surface of the fibers are titanium, oxygen, silver and lanthanum. As it can be seen from Fig. 9, the spectra show peaks originating from, Ti 3p, Ti 3s, C 1s, Ag 3d, Ti 2p, O 1s, Ti 2s and La 3d. Binding energies were referenced to the C1s binding energy at 284.6 eV (Fig. 10a). The peak located at about 529.6 eV is attributed to the O 1s XPS spectra (Fig. 10b), which can be assigned to lattice oxygen O^{2-}. Fig. 10c shows the XPS spectrum of Ti 2p. The Ti 2p1/2 and Ti 2p3/2 spin–orbital splitting are located at binding energies of 464.4 and 458.4 eV, respectively, corresponding to Ti^{4+} in a tetragonal structure [55]. In Fig. 10d, the Ag 3d spectra of La-Ag-TiO_2 consist of two individual peaks at 373.7 and 367.8 eV, which can be attributed to Ag 3d3/2 and Ag 3d5/2 binding energies, respectively. The peaks at 373.7 and 367.8 eV are attributed to Ag^{+}, which indicates that Ag is in the form of Ag^{+} in La-Ag-TiO_2 nanocomposite [55-57]. The peaks of metallic Ag^0 are observed at 368.23 eV and 374.09 eV [55,57]. Hence, it can be concluded that, silver(I) oxide is formed in the La-Ag-TiO_2 nanocomposite, which is in good agreement with XRD results. Fig. 10e shows the XPS spectra for La 3d region of La-Ag-TiO_2. There are two wide peaks centered at 836.9 eV and 853.7 eV, which are attributed to La $3d_{5/2}$ and La $3d_{3/2}$ binding energies, respectively. The binding energies of La 3d5/2 and La 3d3/2 shift to higher energy region compared with the literature values 834.9 eV and 851.8 eV. It might be due to the formation of Ti–O–La bond [58]. It is recognized that the ionic radius of La^{3+} ion (0.115 nm) is larger than that of Ti^{4+} ion (0.068 nm). Therefore, it is difficult for La^{3+} to really enter into the lattice of TiO_2, whereas Ti^{4+} ions can be substituted in the lattice of La_2O_3 to formation a Ti–O–La bond at the interface. The electronegativity titanium of is higher than that of lanthanum, therefore, the electron density of La in the Ti–O–La reduces and the binding energy of La 3d shifts [58].

3.5. BET surface areas analysis

In general, the surface area of the photocatalyst is the most important factor influencing the photocatalytic activity. The surface area of TiO_2, doped and co-doped TiO_2 nanoparticles was determined using the nitrogen gas adsorption method. The BET surface areas of TiO_2, Ag-TiO_2, La-TiO_2, and La-Ag-TiO_2 are 350, 372, 320 and 285 (m^2/g), and pore volumes of the samples are 0.125, 0.132, 0.114 and 0.101 (cm^3/g), respectively (Table 1). It is obvious from the results that all the prepared samples have a very high surface area compared to that of Degussa TiO_2 ($51m^2/g$).

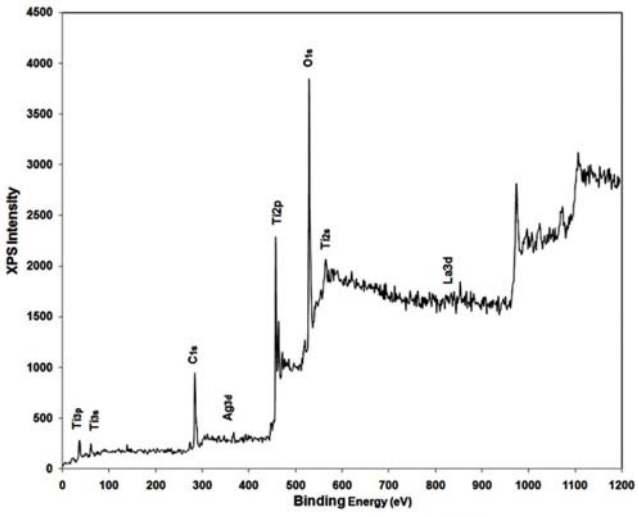

Fig. 9. XPS spectra of La-Ag-TiO_2 nanocomposite.

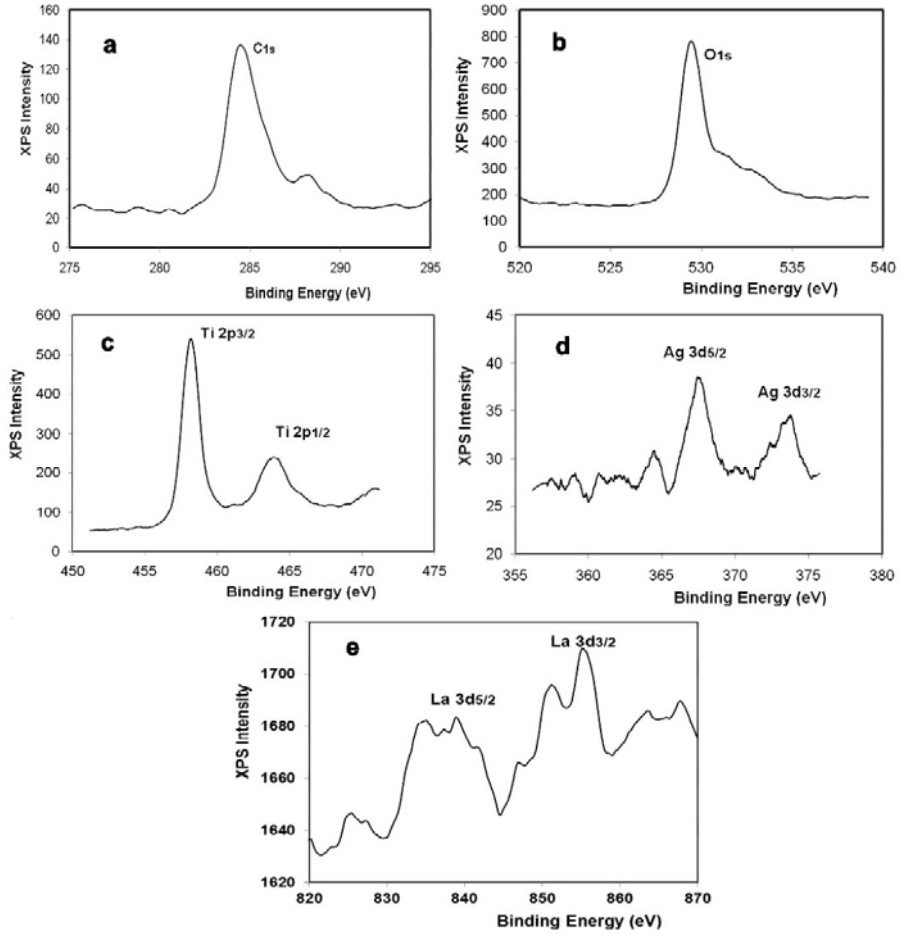

Fig. 10. XPS high resolution spectra of C, O, Ti, La and Ag elements of La-Ag-TiO_2 nanocomposite: (a) C 1s, (b) O 1s, (c) Ti 2p, (d) Ag 3d and (e) La 3d.

TiO_2 nanoparticles have an average particle size of 10-15 nm and BET surface area of about 350 $m^2.g^{-1}$, while Ag-TiO_2 nanoparticles show a diameter of <5 nm, and BET surface area about 372 $m^2.g^{-1}$. Therefore, photoactivity of Ag-TiO_2 nanoparticles onto the surface of fibers is higher than that of TiO_2 nanoparticles. The doping by Ag^+ ion slightly increases the surface area and pore volume of TiO_2, whereas doping by La^{3+} and co-doping process decrease slightly the surface area of La-TiO_2, and La-Ag-TiO_2. The BET surface area of the La-TiO_2 and La-Ag-TiO_2 samples decreases to about 320 and 285 m^2/g, indicating that doping of La^{3+} ion might result in the agglomeration of the nanoparticles which is in the agreement with the TEM result. This result corroborates the possibility of mesoporous nature of the prepared TiO_2 and TiO_2 nanocomposites.

3.6. Photocatalytic self-cleaning activity

The photocatalytic self-cleaning properties of TiO_2, doped and co-doped TiO_2 nanocomposites on fibers were investigated by exposing the coated fibers containing adsorbed MB (cationic dye) and EY (anionic dye) to UV-Vis light. These dyes have strong adsorption characteristics on many surfaces, good resistance to light degradation and direct photolysis, and well-defined optical absorption maxima in the visible region. MB is a kind of basic dye, which is usually used to dye wool, cotton, silk, acrylic etc. When it is used uncontrollably, it can cause serious illness, such as vomiting, sweating and mental disorder [59]. Therefore, MB and EY was chosen as a model contamination to evaluate the photocatalytic activity of the products in this work.

All samples coated with TiO_2, doped and co-doped TiO_2 nanocomposites illustrated a decomposing effect on the dyes upon UV-Vis irradiation. The UV–Vis spectra obtained from the coated samples with dyes prior to and after illumination were recorded. The photodegradation of dyes on the undoped, doped and co-doped TiO_2 nanocomposites deposited on the surface of fabrics was followed by dyes concentration changes (C/C_o) as a function of UV–Vis irradiation time.

For the comparison of reaction rate, the first-order kinetic model was introduced, $lnC/C_o=-kt$, where C is the change of dye concentration at time t, k is the reaction rate constant and C_o is the initial concentration. The degradation rate of the dyes adsorbed on the TiO_2-covered fibers was improved compared to that of the pristine fibers (Fig. 11a, Fig. 11b, Fig. 12a and Fig. 12b). It was observed that the addition of Ag^+ and La^{3+} enhanced the efficiency of the photocatalytic degradation over TiO_2 comparing with the TiO_2 coated fibers (Fig. 11c, Fig. 11d, Fig. 12c and Fig. 12d), while little photocatalytic degradation of dyes was observed on pristine fiber samples.

In particular, La-Ag–TiO_2 shows the highest photocatalytic activity among all the samples (Fig. 11e and Fig. 12e). It can clearly be seen that the self-cleaning property was improved dramatically with increasing of Ag^+ and La^{3+} co doping into the TiO_2 sol. It is found that the photocatalytic activity of coated fibers has the order of La-Ag co-doped TiO_2 > La-doped TiO_2 > Ag-doped TiO_2 > TiO_2, which is in good agreement with the results obtained using the photoluminescence method. As the photodegradation follows the pseudo-first-order reaction, it is worth noting that the dyes degradation rate over co-doped La-Ag/TiO_2 coated on fibers was greater than that of pure and mono-doped TiO_2 (Table 1). Therefore, the k value of the co-doped la-Ag/TiO_2 sample is the largest, which is in accord with the photocatalytic activity.

Photocatalytic self-cleaning mechanism of La-Ag-TiO_2 coated fibers can be explained as follows. When the TiO_2 and/or doped TiO_2 is illuminated by UV-Vis irradiation, a valance band electron (VB) goes to the conduction band (CB) and leaving a hole in the valance band. Subsequently, these electrons are captured by the adsorbed O_2 to give $O_2^{\bullet}$- and the water molecules adsorbed on the surface of the catalyst react with the hole (+) vacancies to give $OH^{\bullet}$. Finally, these active oxygen species attack the dye molecules and decompose them. However, the presence of 'La' and 'Ag' traps the electron from the CB of TiO_2 simultaneously, which suppresses the photo-excited electron–hole recombination.

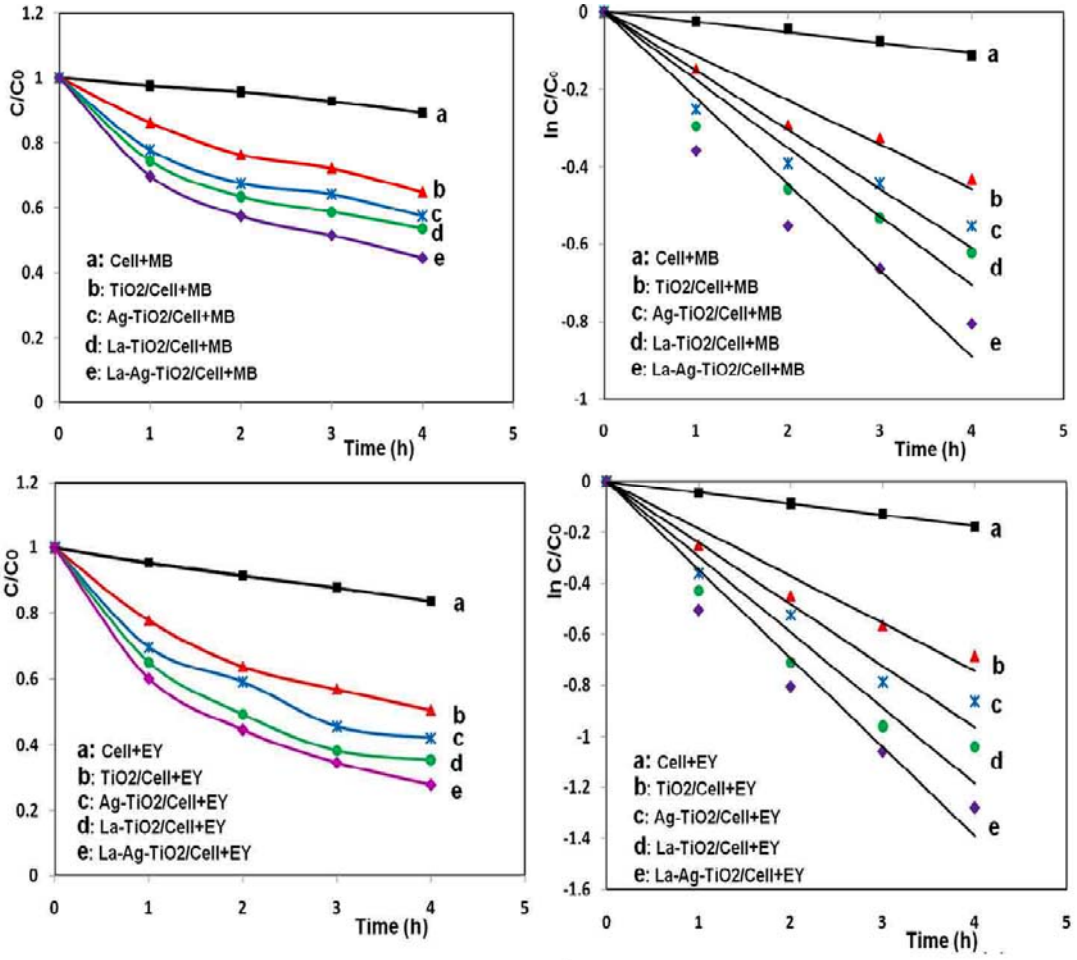

Fig. 11. Photocatalytic decomposition rate of MB and EY on cellulosic fiber against irradiation time. (a) MB and EY on untreated fiber (b) MB and EY on TiO_2 coated fiber (c) MB and EY on Ag-TiO_2 coated fiber (d) MB and EY on La-TiO_2 coated fiber and (e) MB and EY on La-Ag-TiO_2 coated fiber.

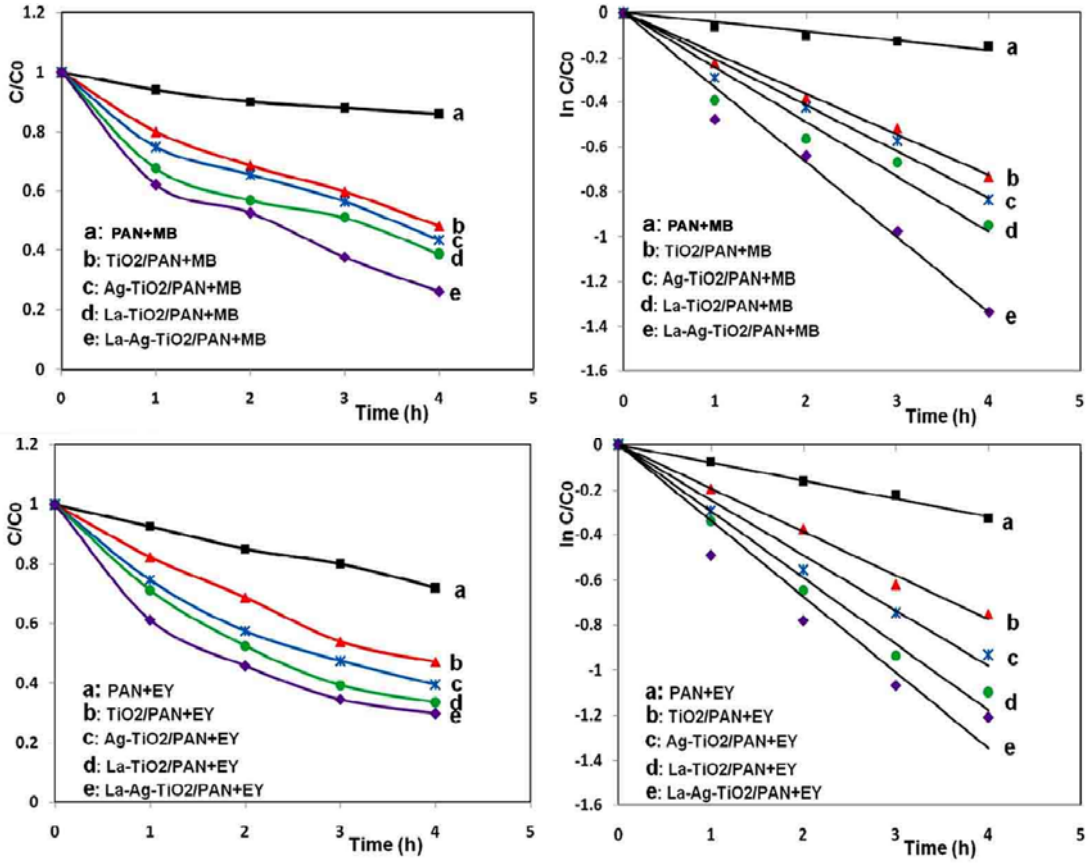

Fig. 12. Photocatalytic decomposition rate of MB and EY on polyacrylonitrile fiber against irradiation time. (a) MB and EY on untreated fiber (b) MB and EY on TiO_2 coated fiber (c) MB and EY on Ag-TiO_2 coated fiber (d) MB and EY on La-TiO_2 coated fiber and (e) MB and EY on La-Ag-TiO_2 coated fiber.

The proposed mechanism is as follows.

(a) Absorption of energy

TiO_2 (or doped TiO_2)+ $h\nu \rightarrow h^+ + e-$ (**1**)

(b) Generation of active oxygen species

$O_2 + e- \rightarrow O_2\bullet-$ (**2**)

$H_2O + h^+ \rightarrow H^+ + OH\bullet$ (**3**)

(c) Oxidation of dyes

Dyes + $O_2\bullet-$ → Degradation products (**4**)

Dyes + $OH\bullet$ → Degradation products (**5**)

The obtained result suggests that the surface modification of TiO_2 with La and Ag improves the photocatalytic activity, which may be attributed not only to the increase in light absorption, but also to the enhancement of charge separation of electron-hole (e–/h+) by trapping photoelectrons. Based on the above results, La and Ag mono-doped TiO_2 has a better performance than pure TiO_2. La^{3+} ions doping can lead to the formation of titanium dioxide lattice distortion, creating oxygen vacancies, which produce shallow states in the bottom of the conduction band to serve as trap sites in TiO_2 [37,39,42]. The shallow energy states introduced by La^{3+} ions in the top valence band serve as hole trap sites. Furthermore, La^{3+} ion has an empty orbital ($4f^0 5d^0 6s^0$), which is relatively stable, and holes trapped can be easily released. So, the charge carriers transfer the life of photo-excited electrons and holes elongate on the surface of the photocatalyst, thus promoting the photoactivity of La-TiO_2 [39,42].

The higher photoactivity of Ag-TiO_2 coated fibers are related to the presence of silver atoms, which are accountable for transferring more photo-generated carriers to the surface and enhance the photocatalytic efficiency [39, 26]. Ag^+ doping can effectively reduce the recombination of electrons and holes through trapping electrons. It is recognized that Ag^+ ion has a unique electronic configuration ($4d^{10}5s^0$), which is relatively stable, and electrons trapped can be easily released, so it prolongates the life of photo-excited carriers [39]. When TiO_2 and Ag with different work functions get in contact (work function of Ag> TiO_2), the schottky barrier will be created and electrons will move from the TiO_2 to the silver atoms. Thus, Silver atoms act as electron traps that conquest photoelectrons produced by light irradiation and increase the separation between photo-generated carriers [26].

The La-Ag co-doped TiO_2 exhibits the highest photocatalytic activity, because La^{3+} and Ag^{+} co-doping are able to effectively decrease the recombination electrons and holes. La^{3+}/Ag^{+} co-doping is more beneficial than single doping to the photocatalytic activity of TiO_2 film, which is believed to be due to the synergistic effect between the La and Ag doped into TiO_2 lattice. A strong La-Ag synergistic interaction appears to play a decisive role for the outstanding photocatalytic self-cleaning performance of La-Ag co-doped TiO_2 by affecting on the electronic properties, the surface microstructure and surface properties.

4. Conclusions

To enhance the photocatalytic activity of TiO_2 on surface fibers, La–Ag co-doped TiO_2 nanocomposite coating was synthesized on cellulosic and PAN fibers through a sol gel method. The fibers coated with nanocomposites of La-TiO_2, Ag-TiO_2, and La–Ag-TiO_2 show improved photodecomposition of dyes for self-cleaning applications. The obtained materials maintained the anatase phase and a large surface area. Evaluated by photodecomposition of MB and EY dyes photocatalytic activity of La–Ag co-doped TiO_2 was obviously higher than that of pure TiO_2 and mono doped TiO_2 nanocomposites. La and Ag co-doped TiO_2 significantly decrease PL intensity compared with that of single doped TiO_2. The excessive activity of the co-doped La–Ag TiO_2-coted fibers is attributed to the synergistic effect of La and Ag doped into TiO_2 lattice. Such a strong synergistic effect is supposed to be related to both the structural and electronic properties of the photoactive anatase phase and effective inhabitation of the recombination of photo-generated electrons and holes and creation of an increased concentration of active radical species. These results clearly indicate that modification of semiconductor photocatalyst by co-doping process is an effective method for improving the photocatalytic activity.

Acknowledgment

The research was supported by University of Guilan. The authors are greatly thankful to University of Guilan for providing financial assistance of this research project.

References

[1] L. Zhou, J. Deng, Y. Zhao, W. Liu, L. An, F. Chen, Mater. Chem. Phys. 117 (2009) 522-527.
[2] K. Huo, B. Gao, J. Fu, L. Zhaod, P. K. Chu, RSC Adv. 4 (2014) 17300-17324.
[3] F. Li, X. Wang, Y. Zhao, J. Liu, Y. Hao, R. Liu, D. Zhao, Appl. Catal. B 144 (2014) 442-453.
[4] Y.J. Xu, J. X. Liao, Q.W. Cai, X.X. Yang, Sol. Energy Mater. Sol. Cells. 113 (2013) 7-12.
[5] H.F. Moafi, A.F. Shojaie, M.A. Zanjanchi, J. Appl. Polym. Sci. 118 (2010) 2062-2070.
[6] H.F. Moafi, A.F. Shojaie, M.A. Zanjanchi, Appl. Surf. Sci. 256 (2010) 4310-4316.
[7] M. Saif, S.A. El-Molla, S.M.K. Aboul-Fotouh, H. Hafez, M.M. Ibrahim, M.S.A. Abdel-Mottaleb, L.F.M. Ismail, Spectrochim. Acta Part A. 112 (2013) 46-51.
[8] D. Wu, M. Long, J. Zhou, W. Cai, X. Zhu, C. Chen, Y. Wu, Surf. Coat. Tech. 203 (2009) 3728-3733.
[9] J. Yang, Y. Han, J. Choy, Thin Solid Films. 495 (2006) 266-271.
[10] E. Pakdel, W.A. Daoud, X. Wang, Appl. Surf. Sci. 275 (2013) 397-402.
[11] A.A. Ismail, H. Bouzid, Colloid Interface Sci. 404 (2013) 127-134.
[12] M.H. Habibi, E. Askari, Iran. J. Catal. 1 (2011) 41-44.
[13] O. Kesmez, H.E.C.E. Burunkaya, E. Arpac, Sol. Energy Mater. Sol. Cells. 93 (2009) 1833–1839
[14] R. Prado, G. Beobide, A. Marcaide, J. Goikoetxea, A. Aranzabe, Sol. Energy Mater. Sol. Cells. 94 (2010) 1081–1088.
[15] N. Sobana, M. Muruganadham, M. Swaminathan, J. Mol. Catal. A: Chem. 258 (2006) 124–132.
[16] M. Rehan, A. Hartwig, M. Ott, L. Gätjen, R. Wilken, Surf. Coat. Technol. 219 (2013) 50–58.
[17] G.C. Collazzo, E.L. Foletto, S.L. Jahn, M.A. Villetti, J. Environ. Manage. 98 (2012) 107-111.
[18] X. Lin, F. Rong, D. Fu, C. Yuan, Powder Technol. 219 (2012) 173–178.
[19] Y. Liu, J. Liu, Y. Lin, Y. Zhang, Y. Wei, Ceram. Int. 35 (2009) 3061–3065.
[20] K. Umar, M.M. Haque, M. Muneer, T. Harada, M. Matsumura, J. Alloys Compd. 578 (2013) 431–438.
[21] J. Xie, D. Jiang, M. Chen, D. Li, J. Zhu, X. Lü, C. Yan, Colloids Surf. A 372 (2010) 107–114.
[22] Y. Zhang, Q. Li, Solid State Sci. 16 (2013) 16-20.
[23] T. Ando, T. Wakamatsu, K. Masuda, N. Yoshida, K. Suzuki, S. Masutani, I. Katayama, H. Uchida, H. Hirose, A. Kamimoto, Appl. Surf. Sci. 255 (2009) 9688–9690.
[24] M. Bordbar, S.M. Vasegh, S. Jafari, A.Y. Faal, Iran. J. Catal. 5 (2015) 135-141.
[25] X. Yin, W. Que, Y. Liao, H. Xie, D. Fei, Colloids Surf. A 410 (2012) 153–158.
[26] X. Hou, M. Huang, X. Wu, A. Liu, Chem. Eng. J. 146 (2009) 42–48.
[27] L.G. Devi, B. Nagaraj, K.E. Rajashekhar, Chem. Eng. J. 181–182 (2012) 259–266.
[28] C. Suwanchawalit, S. Wongnawa, P. Sriprang, P. Meanha, Ceram. Int. 38 (2012) 5201–5207.
[29] P.S.S. Kumar, R. Sivakumar, S. Anandan, J. Madhavan, P. Maruthamuthu, M. Ashokkumar, Water Res. 42 (2008) 4878–4884.
[30] G.K. Naik, P.M. Mishra, K. Parida, Chem. Eng. J. 229 (2013) 492–497.
[31] J. Fang, S. Cao, Z. Wang, M.M. Shahjamali, S.C.J. Loo, J. Barber, C. Xue, Int. J. Hydrogen Energy. 37 (2012) 17853 -17861.
[32] B. Wang, C. Li, H. Cui, J. Zhang, J. Zhai, Q. Li, Chem. Eng. J. 223 (2013) 592–603.

[33] S. Kim, S. Lee, J. Photochem. Photobiol. A 203 (2009) 145–150.
[34] L. Vafayi, S. Gharibe, Iran. J. Catal. 5 (2015) 365-371.
[35] K. Rajkumar, P. Vairaselvi, P. Saravanan, V.T.P. Vinod, M. Cernikc, R.T. Rajendra Kumar, RSC Adv. 5 (2015) 20424-20431.
[36] G. Yang, Z. Jiang, H. Shi, M.O. Jonesb, T. Xiao, P.P. Edwardsb, Z. Yan, Appl. Catal. B 96 (2010) 458–465.
[37] Q. Wang, S. Xu, F. Shen, Appl. Surf. Sci. 257 (2011) 7671–7677.
[38] R. Khana, S. Kima, T. Kima, C. Nam, Mater. Chem. Phys. 112 (2008) 167–172.
[39] N. Zhao, M. Yao, F. Li, F. Lou, J. Solid State Chem. 184 (2011) 2770–2775.
[40] T. Sun, J. Fan, E. Liu, L. Liu, Y. Wang, H. Dai, Y. Yang, W.H. X. Hu, Z. Jiang, Powder Technol. 228 (2012) 210–218.
[41] X. Zhang, Q.Q. Liu, Appl. Surf. Sci. 254 (2008) 4780–4785.
[42] Z. Shi, X. Zhang, S. Yao, Particuology 9 (2011) 260–264.
[43] F.Y. Wei, L.G. Ni, P. Cui, J. Hazard Mater. 156 (2008) 135–140.
[44] S. Zhang, Ultrason. Sonochem. 19 (2012) 767–771.
[45] N. Yao, C. Wu, L. Jia, S. Han, B. Chi, J. Pu, L. Jian, Ceram. Int. 38 (2012) 1671–1675.
[46] X. Zhou, B. Jin, S. Zhang, H. Wang, H. Yu, F. Peng, Electrochem. Commun. 19 (2012) 127–130.
[47] L. Gomathi Devi, B. Nagaraj, K. Eraiah Rajashekhar, Chem. Eng. J. 181–182 (2012) 259–266.
[48] M.A. Moharram, T.Z.A.E. Nasr, N.A. Hakeem, J. Polym. Sci. Polym. Lett. 19 (1981) 183–187.
[49] P.J. Sanchez-Soto, M.A. Aviles, J.C. del Rio, J.M. Gines, J. Pascual, J.L. Perez-Rodr´iguez, J. Anal. Appl. Pyrol. 58–59 (2001) 155–172.
[50] Z.H. Dhoondia, H. Chakraborty, Nanomater. Nanotech. 2 (2012) 1-7.
[51] R. Janardhanan, M. Karuppaiah, N. Hebalkar, T.N. Rao, Polyhedron 28 (2009) 2522–2530.
[52] X. Wang, S. Li, H. Yu, J. Yu, S. Liu, Chem. Eur. J. 17 (2011) 7777-7780.
[53] N. Venkatachalam, M. Palanichamy, V. Murugesan, J. Mol. Catal. A 273 (2007) 177–185.
[54] Y.X. Zhang, G.H. Li, Y.X. Jin, Y. Zhang, J. Zhang, L.D. Zhang, Chem. Phys. Lett. 365 (2002) 300–304.
[55] Y. Zhang, Z. Tang, X. Fua, Y. Xu, Appl. Catal. B 106 (2011) 445–452.
[56] D. Wu, M. Long, ACS Appl. Mater. Interfaces 3 (2011) 4770–4774.
[57] P. Wang, B. Huang, X. Qin, X. Zhang, Y. Dai, M. Whangbo, Inorg. Chem. 48 (2009) 10697-10702.
[58] Y. Cong, B. Tian, J. Zhang, Appl. Catal. B 101 (2011) 376–381.
[59] A. Nezamzadeh-Ejhieh, H. Zabihi-Mobarakeh, J. Ind. Eng. Chem. 20 (2014) 1421–1431.